

The Lipkin-Meshkov-Glick model as a particular limit of the $SU(1, 1)$ Richardson-Gaudin integrable models

S. Lerma H.^a, J. Dukelsky^b

^a*Departamento de Física, Universidad Veracruzana, Xalapa, 91000, Veracruz, Mexico*

^b*Instituto de Estructura de la Materia, C.S.I.C., Serrano 123, E-28006 Madrid, Spain*

Abstract

The Lipkin-Meshkov-Glick (LMG) model has a Schwinger boson realization in terms of a two-level boson pairing Hamiltonian. Through this realization, it has been shown that the LMG model is a particular case of the $SU(1, 1)$ Richardson-Gaudin (RG) integrable models. We exploit the exact solvability of the model to study the behavior of the spectral parameters (pairons) that completely determine the wave function in the different phases, and across the phase transitions. Based on the relation between the Richardson equations and the Lamé differential equations we develop a method to obtain numerically the pairons. The dynamics of pairons in the ground and excited states provides new insights into the first, second and third order phase transitions, as well as into the crossings taking place in the LMG spectrum.

Keywords: Richardson-Gaudin models, Lipkin-Meshkov-Glick model, Quantum phase transitions, Integrable models

1. Introduction

The LMG model was introduced in nuclear physics to mimic the behavior of closed shell nuclei [1]. It is a simple model with one quantum degree of freedom. The dimension of the Hamiltonian matrix increase linearly with the size of the systems allowing its exact diagonalization for large system sizes. As such, the model has been extremely useful to test many-body approximations to nuclear problems (see for example [2] and references therein). More recently the model found applications to many other areas of physics like quantum spin systems [3], ion traps [4], Bose-Einstein condensates in double wells [5] or in cavities [6], and in circuit QED [7]. The model has been also utilized to study quantum phase transitions (QPT) [8, 9] and their relations with quantum entanglement properties [10, 11], as well as to explore excited states QPT [12] and quantum decoherence [13]. On a different respect, the LMG model was shown to be exactly solvable [14] and quantum integrable [15] as a particular limit of the $SU(1, 1)$ Richardson-Gaudin integrable models [16, 17]. The most important feature of the exact solution is that it provides a unique form for the wavefunction of the complete set of eigenstates of the model in terms of a set of pair energies or pairons obtained as a solution of the non-linear coupled Richardson equations. The distribution of pair energies in the energy space change dramatically close to a critical point. A typical example is the exactly solvable $p_x + ip_y$ fermion superfluid derived from the $SU(2)$ hyperbolic RG model [18, 19, 20]. The model has two interesting lines in the phase diagram of density versus coupling constant: a) the Moore-Read line in which all pairons collapses to zero energy, and b) the Read-Green line in which all pairons are real and negative. While in the first case the existence of a QPT is still debated, in the second case it has been shown that Read-Green line corresponds to a third order QPT.

The LMG can be mapped to a two-level boson systems by means of the Schwinger representation of the $SU(2)$ algebra. In this representation the LMG Hamiltonian transforms to a two-level boson pairing

Email addresses: slerma@uv.mx (S. Lerma H.), dukelsky@iem.cfmac.csic.es (J. Dukelsky)

model associated with a $SU(1,1) \otimes SU(1,1)$ algebra [14]. Within these models, the relation between the distribution of pair energies and the occurrence of a QPT has been discussed in Ref. [21] in connection with the s - d dominance in the Interacting Boson Model of nuclear physics. More recently, a thorough analysis of critical points of the two-site Bose-Hubbard model in terms of the roots of the Richardson equations has been presented [22], showing the intimate relation between quantum criticality and the rapid change in the behavior of the pairons. In this paper we will continue these studies focusing on the generalized LMG model which has a rather rich phase diagrams with lines of first and second order QPT and a triple point with a third order QPT. Moreover, the pair energies in a region of the parameter space display a behavior similar to the $p_x + ip_y$ superfluid model, opening the possibility of correlating the physics of both models in the critical regions.

We will start by introducing the LMG model, its Schwinger boson representation leading to a two-level boson pairing model, and the mean field phase diagram of the model in section 2. In section 3 we will introduce the $SU(1,1)$ RG models and discuss the limits leading to the LMG model. We will introduce in this section a robust numerical method to solve the Richardson equations based on their relation with the Lamé ordinary differential equation. Section 4 is devoted to the study of the behavior of the ground state pairons close to the phase transition, and the region in parameters space which shows a behavior similar to the $p_x + ip_y$ model. Finally, in section 5 we will describe the RG solutions for the excited states. Concluding remarks are given in section 6.

2. The Lipkin-Meshkov-Glick model and its bosonic representation

The LMG model is based on the $SU(2)$ algebra, whose three elements satisfy the commutation relations

$$[S_+, S_-] = 2S_z, \quad [S_z, S_\pm] = \pm S_\pm.$$

The three elements can be considered as the components of the pseudo-spin operator \mathbf{S} . They commute with the Casimir operator of $SU(2)$, $\mathbf{S}^2 = \frac{1}{2}(S_+S_- + S_-S_+) + S_z^2$. In terms of these elements the LMG Hamiltonian can be written as

$$H_L = \epsilon S_z + \frac{\lambda}{2} (S_+^2 + S_-^2) + \frac{\gamma}{2} (S_+S_- + S_-S_+), \quad (1)$$

Note that H_L does not commute with the z component S_z for $\lambda \neq 0$ but it commutes with the total pseudo-spin Casimir operator \mathbf{S}^2 . Therefore, the Hilbert space of the model can be separated in different sub-spaces labeled by the eigenvalues of the total pseudo-spin $j(j+1)$, with basis $\mathcal{H}_j = \{|jm\rangle : m = -j, -j+1, \dots, j-1, j\}$. Additionally, the LMG Hamiltonian commutes with the parity operator $\hat{P} = \exp i\pi(S_z + j)$, yielding, for a given j , two invariant sub-spaces ($P = +$ and $P = -$), which are spanned, respectively, by the basis $\mathcal{H}_{j+} = \{|jm\rangle : m = -j, -j+2, -j+4, \dots\}$ and $\mathcal{H}_{j-} = \{|jm\rangle : m = -j+1, -j+3, -j+5, \dots\}$. From now on and for the sake of simplicity, we will assume integer values for j . The semi-integer case can be worked out following the same lines with some slight modifications. For integer j the dimensions of the invariant subspaces, \mathcal{H}_{j+} and \mathcal{H}_{j-} , are $j+1$ and j respectively.

Having introduced the LMG Hamiltonian in terms of $SU(2)$ operators, a physical realization of the model requires a representation of the algebra either in terms of a collection of spins or in terms of a fermionic or bosonic system. In its original presentation the $SU(2)$ operators were expressed in terms of a collection of $2j$ fermions distributed in two levels, each having a $2j$ fold degeneracy. Instead we will make use of the Schwinger boson representation of the $SU(2)$ which allows to a simple connection with the bosonic RG integrable models.

The Schwinger representation of the $SU(2)$ algebra in terms of two bosons is

$$S_z = \frac{b^\dagger b - a^\dagger a}{2} = \frac{\hat{n}_b - \hat{n}_a}{2}, \quad S_+ = b^\dagger a, \quad S_- = a^\dagger b, \quad (2)$$

with a and b boson operators, satisfying the usual commutation rules $[a, a^\dagger] = [b, b^\dagger] = 1$ and $[a, b] = [a, b^\dagger] = 0$. Inserting the boson mapping (2) into the Hamiltonian (1) the bosonic version of the LMG Hamiltonian reads:

$$H_L = \frac{\gamma + \epsilon}{2} b^\dagger b + \frac{\gamma - \epsilon}{2} a^\dagger a + \frac{\lambda}{2} (b^\dagger a^2 + a^\dagger b^2) + \gamma (b^\dagger a^\dagger ab). \quad (3)$$

Using the Schwinger representation, a basis for the Hilbert space with total pseudo-spin j can be written in terms of boson creation operators as $|jm\rangle = |n_a = j - m, n_b = j + m\rangle$, where $|n_a, n_b\rangle = \frac{(a^\dagger)^{n_a} (b^\dagger)^{n_b}}{\sqrt{n_a! n_b!}} |0\rangle$, with $|0\rangle$ the boson vacuum. Note that for a given j the total number of bosons is constant $N \equiv n_b + n_a = 2j$. Likewise, the positive and negative parity basis in the Schwinger representation are given by"

$$\mathcal{H}_{j+} = \{|n_a = 2j, n_b = 0\rangle, |n_a = 2j - 2, n_b = 2\rangle, |n_a = 2j - 4, n_b = 4\rangle, \dots\}$$

$$\mathcal{H}_{j-} = \{|n_a = 2j - 1, n_b = 1\rangle, |n_a = 2j - 3, n_b = 3\rangle, |n_a = 2j - 5, n_b = 5\rangle, \dots\}.$$

A detailed analysis of the LMG phase diagram in terms $SU(2)$ coherent states with definite parity has been performed in Ref. [8]. The different phases of the model and the order of their transitions were identified. Here we repeat that analysis using the Schwinger representation and the boson coherent state

$$|z_a z_b\rangle = e^{-\frac{|z_a|^2 + |z_b|^2}{2}} e^{z_a a^\dagger + z_b b^\dagger} |0\rangle, \quad (4)$$

where z are c-numbers parametrized as $z = \rho e^{i\theta}$. The expectation value of the LMG Hamiltonian (3) in the coherent state $|z_a z_b\rangle =$ is

$$\langle z_b z_a | H_L | z_a z_b \rangle = \frac{\gamma + \epsilon}{2} \rho_b^2 + \frac{\gamma - \epsilon}{2} \rho_a^2 + (\lambda \cos(2(\theta_a - \theta_b)) + \gamma) \rho_a^2 \rho_b^2. \quad (5)$$

The constraint $n_a + n_b = 2j$ implies that coherent states parameters should fulfilled $\rho_a^2 + \rho_b^2 = 2j$. Enforcing this relation, the energy surface is

$$E[\rho_b, \theta] = \langle z_b z_a | H_L | z_a z_b \rangle = \frac{2j\epsilon}{2j-1} \left[A + (2j-1 + jB_\theta) \left(\frac{\rho_b^2}{2j} \right) - jB_\theta \left(\frac{\rho_b^2}{2j} \right)^2 \right], \quad (6)$$

with $A = \frac{\gamma_x + \gamma_y - 2(2j-1)}{4}$ and $B_\theta = (\gamma_x + \gamma_y + (\gamma_x - \gamma_y) \cos 2\theta)$, where we have used $\theta = \theta_a - \theta_b$, and the re-scaled parameters defined in [8]

$$(\gamma_x, \gamma_y) \equiv \frac{2j-1}{\epsilon} (\gamma + \lambda, \gamma - \lambda). \quad (7)$$

In the thermodynamic limit, $j \rightarrow \infty$, the energy per particle, $\mathcal{E}[\rho_b, \theta] \equiv E[\rho_b, \theta]/(2j)$, simplifies to

$$\frac{2\mathcal{E}[\rho_b, \theta]}{\epsilon} + 1 = (2 + B_\theta) \left(\frac{\rho_b^2}{2j} \right) - B_\theta \left(\frac{\rho_b^2}{2j} \right)^2, \quad (8)$$

where terms of order $\mathcal{O}(1/j)$ have been neglected. The phase diagram of the LMG model is obtained by minimizing the energy (8) with respect to the variables $\theta \in (-\pi, \pi)$ and $\frac{\rho_b^2}{2j} \in [0, 1]$ for different values of the model parameters, $\gamma_x - \gamma_y$. The different phases, separated by dashed lines in Fig.1, are described in Table I where we have classified the values of the parameters θ and ρ_b characterizing the coherent state (4) at the absolute minimum. Additionally, Table I shows the energy per particle and the expectation values of the operators S_x^2 and S_y^2 that play the role of order parameters. The critical line $\gamma_x = \gamma_y < -1$ is a special case because the relative phase θ is completely undetermined, i.e. the minimum in energy is independent of θ .

We are now ready to establish the phase diagram of the LMG model in the Schwinger boson representation. In complete accord with Ref.[8], three phases are identified, which are distinguished by the occupation of boson b and the relative phase (θ) of the coherent state parameters z_a and z_b . Alternatively we can characterize the three phases by the order parameters $\frac{\langle S_x^2 \rangle}{j^2} = (\rho_a^2/j)(\rho_b^2/j) \cos^2 \theta$ and $\frac{\langle S_y^2 \rangle}{j^2} = (\rho_a^2/j)(\rho_b^2/j) \sin^2 \theta$, where we have neglected terms of order $\mathcal{O}(1/j)$. Phase A ($\gamma_x \geq -1$ and $\gamma_y \geq -1$) has zero occupation of the

phase	region	θ_{min}	$\left(\frac{\rho_b^2}{2j}\right)_{min}$	$\left(\frac{2\mathcal{E}}{\epsilon} + 1\right)_{min}$	$\left(\frac{\langle S_x^2 \rangle}{j^2}\right)_{min}$	$\left(\frac{\langle S_y^2 \rangle}{j^2}\right)_{min}$
A	$\gamma_y \geq -1$ and $\gamma_x \geq -1$	0	0	0	0	0
B	$\gamma_y > \gamma_x$ and $\gamma_x < -1$	0 or π	$\frac{\gamma_x+1}{2\gamma_x}$	$\frac{(\gamma_x+1)^2}{2\gamma_x}$	$4\left(\frac{\rho_a^2}{2j}\right)\left(\frac{\rho_b^2}{2j}\right)$	0
C	$\gamma_y < \gamma_x$ and $\gamma_y < -1$	$\pm\frac{\pi}{2}$	$\frac{\gamma_y+1}{2\gamma_y}$	$\frac{(\gamma_y+1)^2}{2\gamma_y}$	0	$4\left(\frac{\rho_a^2}{2j}\right)\left(\frac{\rho_b^2}{2j}\right)$

Table 1: Phases and their order parameters in the LMG model

boson b , $\left(\frac{\rho_b^2}{2j}\right)_{min} = \frac{\langle z_a z_b | \hat{n}_b | z_a z_b \rangle}{2j} = 0$. Therefore the two order parameters are also zero, $\langle S_x^2 \rangle = \langle S_y^2 \rangle = 0$. In phase B, ($\gamma_y > \gamma_x$ and $\gamma_x < -1$), the coherent state mixes a and b and the order parameter $\langle S_x^2 \rangle / (j^2)$ is finite. Finally, phase C with ($\gamma_y < \gamma_x$ and $\gamma_y < -1$) is the mirror of phase B corresponding to an exchange between x and y . Upon inspection of the order parameters, we can immediately recognize that the transitions between phases (A-B) and (A-C) are continuous in the order parameters, defining a second order phase transition. The transition between B and C is discontinuous in the order parameters characterizing a first order phase transition. These facts were confirmed in Ref. [8] by analyzing the energy derivatives. At the triple point, $\gamma_x = \gamma_y = -1$, both order parameters converge to 0 avoiding the discontinuity of the first order critical line. As shown in [8] this critical point represents a third order phase transition when it is traversed in the direction indicated by the arrow in Fig.1.

3. $SU(1,1)$ Richardson-Gaudin and LMG models

While the exact solution of the LMG was derived in Ref. [14] using an algebraic approach based on the Bethe ansatz, the connection between the LMG Hamiltonian and the $SU(1,1)$ RG models was established later [15]. In order to make the present work self-contained and to fix the notation, we will here derive the exact solution of the LMG Hamiltonian from the more general $SU(1,1)$ RG models following a different path.

The non-compact $SU(1,1)$ algebra, defined in terms of ladder (K_+, K_-) and weight (K_z) operators resembles that of the $SU(2)$ group, differing in a sign in the commutation relations

$$[K^z, K^\pm] = \pm K^\pm, \quad [K^+, K^-] = -2K^z.$$

Let us now consider N_c different copies of the $SU(1,1)$ algebra, and construct N_c linear and quadratic hermitian combinations of the three elements of the algebra

$$R_i = K_i^z - 2g \sum_{j \neq i} \left[\frac{X(t_i, t_j)}{2} (K_i^+ K_j^- + K_i^- K_j^+) - Z(t_i, t_j) K_i^z K_j^z \right], \quad (9)$$

where i, j label each of the N_c copies and g is an arbitrary parameter. The structure of the operators R_i is such that they commute with the total K^z operator ($K^z = \sum_i K_i^z$). It has been shown [16] that the N_c operators commute among themselves ($[R_i, R_j] = 0$), defining an integrable model, if the functions $X(t_i, t_j)$ and $Z(t_i, t_j)$ are anti-symmetric functions of an arbitrary set of parameters t_i

$$X(t_i, t_j) = \frac{\sqrt{(1+st_i^2)(1+st_j^2)}}{t_i - t_j}, \quad Z(t_i, t_j) = \frac{1+st_it_j}{t_i - t_j}. \quad (10)$$

The parameter s can take three different values $s = 0, 1, -1$, defining the rational, the trigonometric, and the hyperbolic families of $SU(1,1)$ RG models respectively.

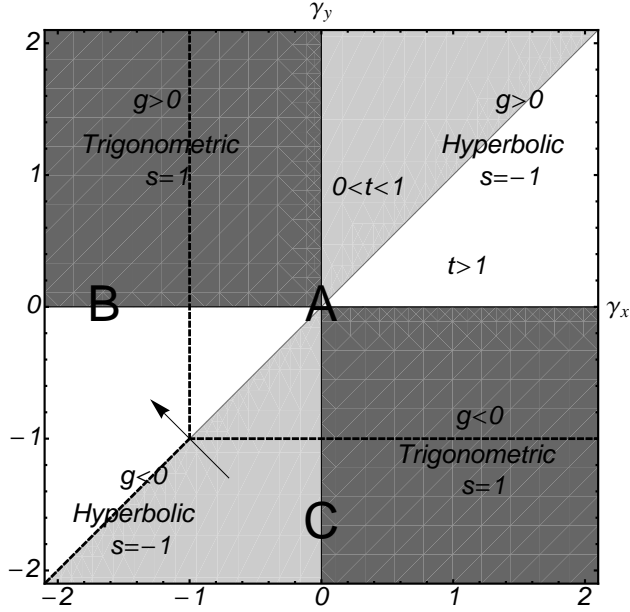


Figure 1: Phase diagram of the LMG model and Richardson-Gaudin areas of integrability in the γ_x - γ_y parameter space. The light quadrants correspond to hyperbolic model ($s = -1$) with light gray for $0 < t < 1$ and white for $t > 1$. Dark gray quadrants correspond to the trigonometric model. Upper quadrants correspond to positive g while lower quadrants to negative g . The dashed lines separate the three different phases (A,B and C) of the LMG model discussed in the text. The triple point $(-1, -1)$ in the intersection of the lines is a third order transitions when it is traversed in the direction indicated by the arrow. The horizontal line $\gamma_y = 0$ and the vertical one $\gamma_x = 0$ correspond to the rational version of the model ($s = 0$).

The LMG model is obtained in the limit of two $SU(1, 1)$ copies, which we will label as a and b . In the pair boson representation of the $SU(1, 1)$ algebra, the elements of the two copies are

$$\begin{aligned} K_a^+ &= \frac{1}{2}a^\dagger a^\dagger & K_a^- &= \frac{1}{2}aa, & K_a^z &= \frac{1}{2}\left(a^\dagger a + \frac{1}{2}\right) \\ K_b^+ &= \frac{1}{2}b^\dagger b^\dagger & K_b^- &= \frac{1}{2}bb, & K_b^z &= \frac{1}{2}\left(b^\dagger b + \frac{1}{2}\right). \end{aligned} \quad (11)$$

The irreducible representations (irreps) of the non-compact $SU(1, 1)$ algebra are dimensionally infinite, but they possess a minimum weight state defined by $K_i^- |MW\rangle = 0$. For the previous bosonic representation, these states are given by $|\nu_i = 0\rangle \equiv |0\rangle_i$ and $|\nu_i = 1\rangle \equiv |1\rangle_i$, where $|0\rangle_i$ is the vacuum of bosons $i = a, b$. The parameters ν_i are the so-called seniorities of each of the $SU(1, 1)$ copies. The seniority quantum number, ν_i , counts the number of unpaired bosons i and can take only two values 0 or 1. If $\nu_i = 0$ the number of bosons i (n_i) is even, and odd if $\nu_i = 1$.

Inserting the boson pair representation of the two copies (11) in the integrals of motion (9) we construct the two integrals of motion of the LMG model. We can verify the the sum of both integrals gives the conserved quantity K^z . Taking the difference between both we obtain:

$$\begin{aligned} R_b - R_a &= K_b^z - K_a^z - 2gX_{ba} [K_b^+ K_a^- + K_a^+ K_b^-] + 4gZ_{ba} K_b^z K_a^z \\ &= \frac{1}{2}(b^\dagger b - a^\dagger a) - g\frac{X_{ba}}{2}(b^{\dagger 2}a^2 + a^{\dagger 2}b^2) + gZ_{ba}\left(b^\dagger b + \frac{1}{2}\right)\left(a^\dagger a + \frac{1}{2}\right), \end{aligned}$$

with $Z_{ba} \equiv Z(t_b, t_a)$ and $X_{ba} \equiv X(t_b, t_a)$. Comparing with the LMG Hamiltonian in the Schwinger representation (3), one finds the following relation between the LMG model and the integrals of motion of the

transition	line	RG parameters
first-order	$\gamma_x = \gamma_y, \gamma_x < -1$	$s = -1 \quad t = 1 \quad (2j-1)g = -1$
second-order	$\gamma_x = -1, \gamma_y > -1$	$s = +1 \quad (2j-1)g = +\frac{1}{t}$
		$s = -1 \quad t > 1 \quad (2j-1)g = -\frac{1}{t}$
second-order	$\gamma_x > -1, \gamma_y = -1$	$s = +1 \quad (2j-1)g = -t$
		$s = -1 \quad t < 1 \quad (2j-1)g = -t$

Table 2: Transition lines in phase diagram γ_x, γ_y and their translation to the RG parameters.

$SU(1,1)$ RG models

$$H_L = \epsilon(R_b - R_a) - \frac{\gamma}{4}, \quad \text{with} \quad gX_{ba} = -\frac{\lambda}{\epsilon}, \quad \text{and} \quad gZ_{ba} = \frac{\gamma}{\epsilon}. \quad (12)$$

Without any loss of generality, we choose the parameters entering in X_{ba} and Z_{ba} as $t_b = -t_a \equiv t$, with $t \geq 0$. The functions X_{ba} and Z_{ba} reduce to $X_{ba} = \frac{1+st^2}{2t}$ and $Z_{ba} = \frac{1-st^2}{2t}$. Then, the relation between the LMG Hamiltonian parameters $(\lambda, \gamma, \epsilon)$ and those of the $SU(1,1)$ RG models are

$$\frac{\lambda}{\epsilon} = -g \frac{1+st^2}{2t}, \quad \frac{\gamma}{\epsilon} = g \frac{1-st^2}{2t}.$$

Or in terms of the γ_x and γ_y parameters (7) we have

$$(\gamma_x, \gamma_y) \equiv \frac{2j-1}{\epsilon} (\gamma + \lambda, \gamma - \lambda) = (2j-1)g \left(-st, \frac{1}{t} \right). \quad (13)$$

The relation between the γ_x and γ_y parameters and those of the RG model classify the quadrants of the phase diagram of Fig.1 in terms of the hyperbolic ($s = -1$) and trigonometric ($s = 1$) RG models. The first ($s = -1, g > 0$) and third ($s = -1, g < 0$) quadrants correspond to the hyperbolic RG model, whereas the second ($s = 1, g > 0$) and fourth ($s = 1, g < 0$) are associated with the trigonometric model. These regions are indicated in Figure 1, by dark gray zones for the trigonometric model and light zones for the hyperbolic one. The rational RG model is limited to the $\gamma_x = 0$ and $\gamma_y = 0$ lines.

The phase transition lines, discussed in the section 2 and shown in Fig. 1 by dashed lines, are translated to the RG parameters in table 2.

The LMG model has symmetries that relates the spectrum of systems in two different points in the parameter space. The first of these symmetries is a point reflection through the origin, and relates systems obtained from a simple change of sign in the parameters $(\gamma_x, \gamma_y) \rightarrow (\gamma'_x, \gamma'_y) = (-\gamma_x, -\gamma_y)$. This change in sign is equivalent to a global sign change in the Hamiltonian, implying that the spectrum of a system is minus the spectrum of the transformed system. In terms of the RG parameter, this transformation corresponds to $g \rightarrow g' = -g$. A second symmetry of the LMG model is a reflection across the line $\gamma_y = \gamma_x$. Two mirror points of the phase diagram symmetrically located around this line have exactly the same energy spectrum, as a result of the invariance of the $SU(2)$ algebra under the canonical transformation $S_+ \rightarrow -iS_+, S_- \rightarrow iS_-, S_z \rightarrow S_z$, corresponding to $b \rightarrow ib, a \rightarrow a$ in the Schwinger boson realization [23]. In terms of the RG parameters, this symmetry implies that systems with parameters related by

$$(g, t) \rightarrow (g', t') = (-sg, 1/t), \quad (14)$$

have the same spectrum.

The $\gamma_y = \gamma_x$ line ($s = -1$ and $t = 1$ in terms of RG parameters), located within the hyperbolic regions of the phase diagram, has the peculiarity that the RG solutions display a singular behavior as it will be shown in section 4. However, the eigenstates along this line can be easily obtained in closed form by resorting, for instance, to the LMG Hamiltonian in terms of pseudospin operators. The condition $\gamma_x = \gamma_y$ implies $\lambda = 0$

and results in the following LMG Hamiltonian

$$H_L = \epsilon \left(S_z + \frac{\gamma_x}{2(2j-1)} (S_+ S_- + S_- S_+) \right) = \epsilon (S_z + g (S^2 - S_z^2)), \quad (15)$$

which commutes with both \mathbf{S}^2 and S_z , and has eigenstates $|jm\rangle$ and eigenvalues

$$E_m = \epsilon \left(m + \frac{\gamma_x}{(2j-1)} (j(j+1) - m^2) \right) = \epsilon (m + g (j(j+1) - m^2)). \quad (16)$$

The conservation of the S_z operator along this critical line allows the existence of real crossings between states of the same parity. These crossings take place when $E_m = E_{m\pm 2}$. For instance, the $P+$ ground state energy for $g = 0$, $E_{m=-j}$, crosses the first $P+$ excited state energy, $E_{m=-j+2}$, when $\gamma_x = \gamma_y = -(2j-1)/(2j-2)$, or in terms of RG model parameter when $s = -1$, $t = 1$ and $g = -1/(2j-2)$.

Having related the two-level $SU(1,1)$ RG models with the LMG model, we can now explore the exact RG solutions in each subspace defined by the number of boson pairs M and seniorities ν_a, ν_b . For integer j the number of Schwinger bosons, $N = n_a + n_b = 2j$, is even, the seniorities are equal, $\nu_a = \nu_b \equiv \nu = 0$ or 1 , and the number of boson pairs is $M = j - \nu$. The seniority sectors $\nu = 0$ and $\nu = 1$ correspond to the two invariant sub-spaces $P = +$ and $P = -$ respectively.

The eigenvalues r_i , of the R_i integrals of motion are [15]

$$r_i = d_i \left(1 + 2 \sum_{\alpha}^M Z(t_i, e_{\alpha}) + 2 \sum_{j \neq i} d_j Z(t_i, t_j) \right),$$

where $d_i = (1/2)(\nu_i + \frac{1}{2})$, Z is the function defined in (10), and e_{α} are the so-called spectral parameters or pairons. Each particular eigenstate is completely defined by a particular M pairon solution of the coupled set of Richardson equations

$$1 + 2 \sum_i d_i Z(e_{\alpha}, t_i) + 2 \sum_{\beta \neq \alpha}^M Z(e_{\alpha}, e_{\beta}) = 0.$$

For the particular case of the LMG model, with two $SU(1,1)$ copies, $t_b = -t_a = t$, and integer j ($\nu_a = \nu_b = \nu = 0, 1$), the Richardson equations reduce to

$$\frac{1 - 2gs [M + \nu - \frac{1}{2}] e_{\alpha}}{1 + se_{\alpha}^2} + g \left(\nu + \frac{1}{2} \right) \left(\frac{1}{e_{\alpha} + t} + \frac{1}{e_{\alpha} - t} \right) + 2g \sum_{\beta \neq \alpha}^M \frac{1}{e_{\alpha} - e_{\beta}} = 0. \quad (17)$$

The eigenvalues of the LMG Hamiltonian are given by

$$E_L = \epsilon(r_b - r_a) - \frac{\gamma}{4} = g\epsilon \frac{(1 - st^2)}{2t} \nu(\nu + 1) + 2g\epsilon \left(\nu + \frac{1}{2} \right) t \sum_{\alpha} \frac{1 + se_{\alpha}^2}{t^2 - e_{\alpha}^2}. \quad (18)$$

The unnormalized eigenvectors common to the two integrals of motion (R_i) and, consequently, to the LMG Hamiltonian are

$$\prod_{\alpha=1}^M \left(\frac{a^{\dagger} a^{\dagger}}{e_{\alpha} + t} + \frac{b^{\dagger} b^{\dagger}}{e_{\alpha} - t} \right) |\nu_a \nu_b\rangle. \quad (19)$$

The Richardson equations can be interpreted as an electrostatic problem in two-dimensions [24, 25]. In order to make explicitly this connection we rewrite the Richardson equations as

$$\frac{Q_C}{e_{\alpha} - P_C} + \frac{Q_D}{e_{\alpha} - P_D} + \frac{\nu + \frac{1}{2}}{2} \left(\frac{1}{e_{\alpha} + t} + \frac{1}{e_{\alpha} - t} \right) + \sum_{\beta \neq \alpha}^M \frac{1}{e_{\alpha} - e_{\beta}} = 0, \quad (20)$$

with the effective charges Q_C and Q_D

$$\begin{aligned} Q_C &= \frac{1}{4g\sqrt{-s}} - \frac{2j-1}{4} \\ Q_D &= -\frac{1}{4g\sqrt{-s}} - \frac{2j-1}{4}, \end{aligned} \quad (21)$$

located at position $P_C = -1/\sqrt{-s}$ and $P_D = 1/\sqrt{-s}$ respectively. The pairons have a positive unit charge and they are located at positions e_α in the complex plane. Eq.(20) describes the electrostatic interaction of a set of M pairons with positive unit charge in a two dimensional space. The first two terms in (20) describe the electrostatic interaction of the pairons with the two charges Q_C and Q_D . For the trigonometric case ($s = 1$) the effective charges are complex $Q_C = -\frac{2j-1}{4} - \frac{i}{4g}$, $Q_D = Q_C^*$, and they are located in $P_C = i$, $P_D = -i$. Whereas in the hyperbolic case ($s = -1$) both, the charges and their positions, are real, $Q_C = -\frac{2j-1}{4} + \frac{1}{4g}$ and $Q_D = -\frac{2j-1}{4} - \frac{1}{4g}$, located in $P_C = -1$ and $P_D = 1$ respectively. The third term in (20) represents the interaction of the pairons with two charges $\frac{\nu+\frac{1}{2}}{2}$ at positions $\mp t$. Finally, the fourth term corresponds to the mutual repulsion between pairons. Each independent solution of the Richardson equations determines the equilibrium position of the pairons in the complex plane. The electrostatic mapping will be useful to interpret the pairons distribution in each of the quantum phases of the LMG model and the structural changes that take place close to the quantum phase transitions.

3.1. The Richardson solution as the roots of a generalized Heine-Stieltjes polynomial

The standard way to solve the Richardson equations is to start from the weak coupling limit where the solution is known [see Eq. (33) below]. The coupling strength g is increased gradually, using the previous solution as an initial guess to solve the equations for the updated g by means of a standard Newton-Raphson method. A recursive use of this strategy allows to reach the solution for an arbitrary value of g provided one is able to develop a method to treat the numerical instabilities appearing when two or more pairons converge at the same point (at the position of the t_i parameters in this case) generating singularities in the equations [26]. Recently, two related methods for solving the Richardson equations have been presented ([27, 28] and [29]). Both methods exploit the relation between the Richardson equations and the Lamé's Ordinary Differential Equation which has a generalized form of the Heine-Stieltjes polynomials as a solution. The roots of these polynomials are precisely the spectral parameters or pairons. These methods have the advantage of being numerically more stable for system of moderate sizes. For larger systems they have instabilities due to the large precision needed to calculate the roots of a polynomial of high degree. Here we follow the method of references [27, 28], which is more adequate for systems with a small number of levels [30], as it is the case of the LMG model.

We begin with the Richardson equations in the form (20), which can be written as

$$\sum_{\beta \neq \alpha} \frac{1}{e_\alpha - e_\beta} = - \sum_{k=1}^4 \frac{\rho_k}{e_\alpha - \eta_k}, \quad (22)$$

with $(\rho_k, \eta_k) = (Q_C, -1/\sqrt{-s}), (Q_D, 1/\sqrt{-s}), ((2\nu+1)/4, -t)$, and $((2\nu+1)/4, t)$ for $k = 1, 2, 3, 4$ respectively.

Let us now define the polynomial $P(x) = \prod_{\alpha=1}^M (x - e_\alpha)$ which can be expanded in powers of x as

$$P(x) = \sum_k a_k x^k, \quad (23)$$

whose roots are the set $\{e_\alpha\}$ for a particular solution of the Richardson equations. This polynomial is a generalized Heine-Stieltjes polynomial that satisfies the following Lamé's ordinary differential equation (Appendix A):

$$A(x)P''(x) + B(x)P'(x) - V(x)P(x) = 0, \quad (24)$$

where the functions A, B and V are polynomials defined as

$$A(x) = \prod_k^4 (x - \eta_k), \quad B(x) = A(x) \sum_{k=1}^4 \frac{2\rho_k}{x - \eta_k}, \quad \text{and} \quad V(x) = \sum_i 2\rho_k \Lambda(\eta_k) \prod_{l \neq k} (x - \eta_l), \quad (25)$$

with

$$\Lambda(x) \equiv \frac{P'(x)}{P(x)} = \sum_{\alpha} \frac{1}{x - e_{\alpha}}. \quad (26)$$

The polynomials $A(x)$ and $B(x)$ of degree 4 and 3 respectively, depend only on the parameters of the LMG Hamiltonian (13). $V(x)$, the so called Van Vleck's polynomial, is at most of third order and depends on the values $\Lambda(\eta_i)$, which in turn depend on the set of pairons e_{α} ,

$$V(x) = \sum_{i=0}^3 b_i x^i. \quad (27)$$

For a general problem [27], one can insert the polynomials $V(x)$ (27) and $P(x)$ (23) in the ordinary differential equation (24) and, by equating to zero the coefficients at each order in x , one obtains two systems of equations for the coefficients b_i and a_i . The first set of equations is linear allowing a solution in which coefficients b_i are expressed in terms of the a_i , leaving a second set of non-linear equations for the a_i coefficients. Finally, the a_i coefficients determine the polynomial (23) whose roots are the pairons e_{α} of the Richardson equations. For the particular case of the LMG model the first system of linear equations allows to determine the coefficients of the Van Vleck polynomial b_i (except b_0) directly in terms of the parameters of the problem (i.e. they are independent of the a_i parameters). As a consequence, the second set of equations is linear in the coefficients a_i . From Eq. (25) we obtain:

$$\begin{aligned} A(x) &= -st^2 + (s - t^2)x^2 + x^4 \\ B(x) &= \frac{-st^2}{g} + [t^2(2j - 1) + s(2\nu + 1)]x + \frac{s}{g}x^2 - 2(M - 1)x^3. \end{aligned} \quad (28)$$

After substitution of these polynomials into the differential equation (24), and from the terms of order $M + 3$, $M + 2$ and $M + 1$, we obtain $b_3 = 0$, $b_2 = -M(M - 1)$ and $b_1 = sM/g$, i.e the Van Vleck polynomial is completely determined except for the order zero coefficient:

$$V(x) = b_0 + \frac{sM}{g}x - M(M - 1)x^2.$$

We can derive the b_0 coefficient and the parameters a_i from the orders 0 to M of the differential equation (24). The result is an eigenvalue equation:

$$\sum_{k'=0}^M D_{kk'} a_{k'} = b_0 a_k \quad \text{with } k = 0, 1, \dots, M,$$

where the matrix $D_{kk'}$ is completely determined by the parameters of the model (t, g, M, ν, s) . Its non-zero matrix elements are given by

$$\begin{aligned} D_{k \ k-2} &= (k - 2)(k - 1 - 2M) + M(M - 1) \\ D_{k \ k-1} &= s(k - M - 1)/g \\ D_{k \ k} &= k((2j - k)t^2 + s(2\nu + k)) \\ D_{k \ k+1} &= -s(k + 1)t^2/g \\ D_{k \ k+1} &= -s(k + 2)(k + 1)t^2. \end{aligned} \quad (29)$$

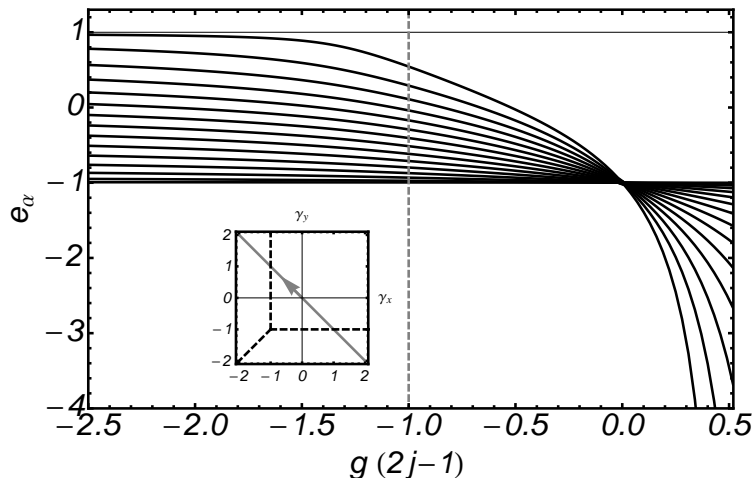


Figure 2: Ground state pairons as a function of $g(2j-1)$ for the trigonometric case ($s = 1$) with $t = 1$ and $j = 15$, corresponding to $\gamma_y = -\gamma_x$ as indicated with the arrow line in the inset. Here the arrow corresponds to increasing values of g . The vertical dashed line indicates the critical value of $g = g_{cr} = -1/(2j - 1)$. Pairons for positive and negative values of g are related by $e_\alpha \rightarrow 1/e_\alpha$.

Therefore, the coefficients a_k of the polynomial $P(x)$ are the elements of each eigenvector of the matrix D . Once the coefficients a_i are known, the e_α roots of the Richardson equations are obtained by finding the roots of the polynomial $P(x)$. Each of the $M + 1$ eigenvectors of matrix D , defines a polynomial whose roots e_α correspond to a particular eigenstate of the LMG Hamiltonian.

It is important to remark here that the drawback or bottleneck of the method resides in the last step. As it is well known, finding the roots of high degree polynomials requires a high precision in the determination of the coefficients. Therefore, the number of pairs M is limited to $\cong 10^2 - 10^3$. Conversely, the method allows to find directly the pairon roots without resorting to the iterative method of increasing gradually the coupling strength with the burden of having to deal with the singularities of the Richardson equations.

4. Numerical Results for the ground state

In this section we will present and discuss the numerical solution of the Richardson equations for the ground state in the different phases using the trigonometric and the hyperbolic model as required for each particular phase.

4.1. Trigonometric quadrants

In order to illustrate typical results for the trigonometric regions ($s = 1$), we will consider the line with $t = 1$ as a function of g . This line corresponds to $\gamma = 0$, which cancels the third term in the LMG Hamiltonian (1). The resulting Hamiltonian is the most frequently used in the literature, also known as the Lipkin Hamiltonian. In terms of the scaled parameters this line corresponds to $\gamma_y = -\gamma_x = (2j - 1)g$. For increasing values of g , we move along the line from the fourth to the second quadrant in the phase diagram. According to this diagram, a second order phase transition takes place in the thermodynamic limit for $\gamma_y = \pm 1$, or equivalently for $g = g_{cr} = \pm 1/(2j - 1)$ (see table 2). The e_α pairons for the ground state as a function of the ratio $g/g_{cr} = g(2j - 1)$ are shown in figure 2, for a system with $j = 15$.

As it can be seen in the figure, for $g \sim 0$ all the pairons are located close to $t = -1$. As the strength of g is increased they expand in the real axis. For negative g , the pairons are constrained to the interval $[-t, t]$, and they behave in a very similar way to the rational case already discussed in the context of the IBM-model [21]. The second order phase transition can be interpreted as a localization-delocalization transition. The pairons initially localized close to $t = -1$, expand to the entire interval $[-t, t]$ in the transition point. For positive g the solutions are, except for a sign in the wave function, entirely equivalent to the negative g

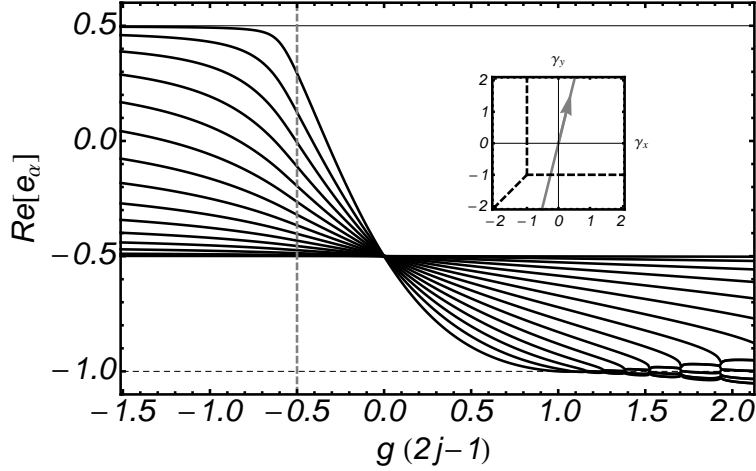


Figure 3: Real part of the ground state pairons as a function of $g(2j-1)$ for the hyperbolic case ($s = -1$) with $t = 1/2$ and $j = 15$, corresponding to $\gamma_y = 4\gamma_x$ as indicated with the arrow line in the inset. The arrow corresponds to increasing values of g . The vertical dashed line indicates the critical value of $g = g_{cr} = -1/(4j-2)$ corresponding to the line $\gamma_y = -1$. For positive g , successive collapses of pairons in the position $P_C = -1$ (horizontal dashed line) of the effective charge Q_C can be seen.

case. As it was discussed in section 3, the Richardson solutions for two mirror points symmetrically located around the $\gamma_x = \gamma_y$ lines [(g, t) and $(-sg, 1/t)$ in terms of RG parameters] have the same spectrum and the wave functions are related by a canonical transformation $b \rightarrow ib$. This symmetry is reflected by a simple relation between the pairons with negative and positive g given by $e_\alpha \rightarrow 1/e_\alpha$. It is straightforward to show that the energy in Eq.(18) is invariant under the transformation $(g, t, e_\alpha) \rightarrow (-sg, 1/t, 1/e_\alpha)$, and that this transformation produces a change in the relative sign of the two terms appearing in the product wave function (19), in agreement with the canonical transformation $b \rightarrow ib$.

In the trigonometric quadrants, the dynamics of the pairons as a function of the control parameters $[\gamma_x, \gamma_y]$ take place entirely in the real axis and it is very much like the already known dynamics of pairons in the rational boson pairing models [21].

4.2. Hyperbolic quadrants

The hyperbolic regions ($s = -1$) of the phase diagram offer much richer structures than the trigonometric regions. In order to illustrate this issue, we will study a system with $j = 15$ and $t = 1/2$, which corresponds to the line $\gamma_y = 4\gamma_x$ in phase diagram of Fig.1. The line traverses the third and first quadrants from below for increasing values of g , and has a critical point of a second order phase transition for $\gamma_y = -1$, corresponding to $g(2j-1) = -t = -1/2$ (see table 2).

Fig. 3 shows the ground state pairon roots as function of $g(2j-1)$. Similarly to the trigonometric results, the pairons converge to $-t$ for $g \rightarrow 0$. For negative values of g the pairons are constrained to the interval $[t, -t]$ with the phase transitions (vertical dashed line) signaled by the delocalization of the pairons in this interval. For the g -positive case (where no phase transition is expected) an interesting behavior of the pairons takes place. As the coupling g is increased the pairons collapse successively to the position ($P_C = -1$) of the effective charge Q_C . In Appendix B it is shown that a necessary condition to have N_C pairons collapsing to $P_C = -1$ is

$$g = g_{N_C}^c \equiv \frac{1}{2j+1-2N_C}, \quad (30)$$

with $N_C = 1, \dots, M$ and $0 < g_{N_C=1}^c < g_{N_C=2}^c < \dots < g_{N_C=M}^c$.

According to this expression, the first collapse occurs for $N_C = 1$ (one collapsing pairon) at $g(2j-1) = g_1^c(2j-1) = 1$, then $N_C = 2$ pairons converge to $P_C = -1$ at $g(2j-1) = g_2^c(2j-1) = (2j-1)/(2j-3)$, and so on. After the collapse of an even number of pairons a new complex conjugated pair of pairons is created. In figure 4, the real and imaginary parts of the pairons are shown for positive g values. The successive collapses

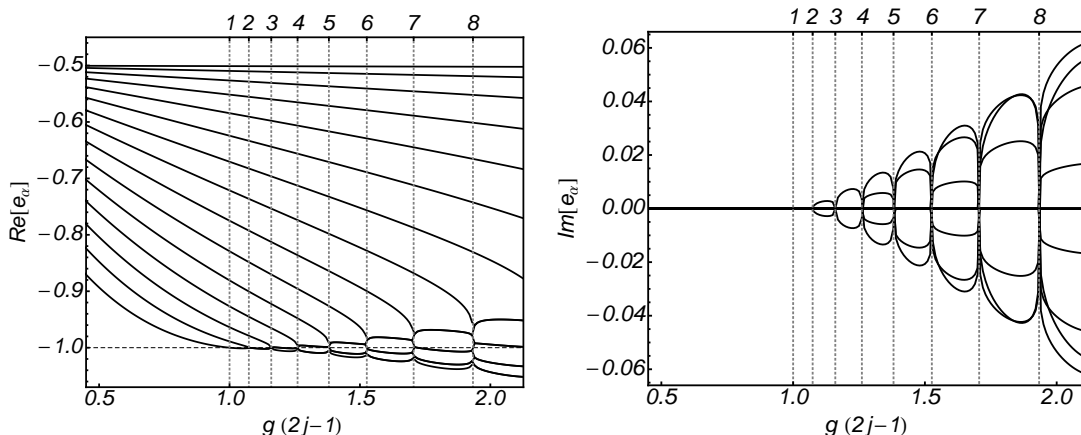


Figure 4: The collapses of the ground state pairons as a function of $g(2j-1)$ for the hyperbolic case of figure 3 ($t = 1/2$ and $j = 15$). Left and right panel show the real and imaginary part of the pairons respectively. The collapses take place in the position $P_C = -1$ (horizontal dashed line in left panel) of the effective charge Q_C at values of g given in (30). The dashed vertical lines indicate the number of pairons $N_C = 1, \dots, 8$ involved in the collapse. After the collapse of an even number of pairons a complex conjugated pair is created as can be seen in the right panel of the figure.

and creation of complex conjugated pairs can be clearly seen. This behavior was completely unexpected in bosonic RG models, where pairons have always been constrained to the real axis.

A particular situation occurs when all pairons collapse to $P_C = -1$ for $g = g_{N_C=j}^c = 1$. At this particular point the exact ground state eigenstate (19) takes the simple form:

$$|\Psi\rangle_{MR} = \left(\frac{a^\dagger a^\dagger}{t-1} - \frac{b^\dagger b^\dagger}{t+1} \right)^j |0\rangle,$$

which would be the boson version of the Moore-Read state found for the $p_x + ip_y$ model [18, 19, 20], derived from the fermionic hyperbolic RG model. Likewise, as in the fermionic model, the energy of this state is $E = 0$. However, within the LMG model it can be shown by exact diagonalization of very large systems that the collapse of all pairons to $P_C = -1$ is not associated with a ground state phase transition. A subject still under debate for the $p_x + ip_y$ fermionic model [18, 19, 20].

It is worth mentioning here that the condition (30) of pairons converging to the value $P_C = -1$ applies equally to the excited states, and that similar collapses in the position ($P_D = +1$) of the effective Q_D charge occurs for excited states in the $g < 0$ interval for values given by

$$g = g_{N_D}^c = -\frac{1}{2j+1-2N_D}, \quad (31)$$

with $N_D = 1, \dots, M$ and $g_{N_D=M}^c < g_{N_D=(M-1)}^c < \dots < g_{N_D=1}^c < 0$. These issues will be discussed in section 5, where it will be shown that, even if the collapses are not associated to a ground state phase transition, they are related to the crossings of excited states of different parities.

4.3. The triple point $\gamma_y = \gamma_x = -1$

The triple point in the phase diagram of the Lipkin model, $(\gamma_x, \gamma_y) = (-1, -1)$, constitutes one of the rare example of a third order phase transition in quantum many-body systems. As such, it deserves a thorough study because it could shed light into other third order QPT like the one taking place in the $p_x + ip_y$ model [20]. The third order character of this phase transition reported in [8] is observed when the critical point is crossed, for instance, along the line $\gamma_y = -\gamma_x - 2$. In figure 5.a the behavior of the ground state pairons close to the triple point is examined for a system of size $j = 10$, moving in the phase diagram along the lines $\gamma_y = -\gamma_x + b$, for three values of b ($b = -2.0$ grey solid line, $b_{cr} = -2.1$ dashed line, and $b = -2.32$

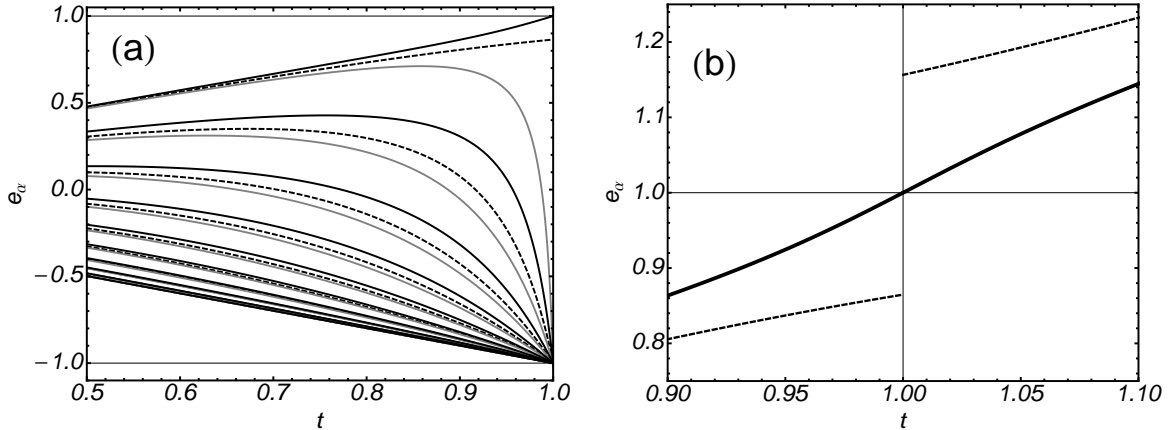


Figure 5: Pairons close to the triple point $(\gamma_x, \gamma_y) = (-1, -1)$ for a $j = 10$ system as a function of t . $t = 1$ corresponds to the line $\gamma_x = \gamma_y$ in the phase diagram. The different lines are associated to three values of values of b along the line $\gamma_y = -\gamma_x + b$. The values $b = -2.0$, $b_{cr} \approx 2.11$ and 2.32 are represented by gray, dashed, and black lines respectively, with $b_{cr} = -2(2j - 1)/(2j - 2)$. Panel (a) describes the behavior of the ten pairons in the interval $0.5 \leq t \leq 1.0$. Panel (b) is a close up of the tenth pairons around $t = 1.0$ showing the discontinuous jump for $b = b_{cr}$.

black solid line). We move along these lines using the parameter t of the RG model (13). The value $t = 1$ corresponds to the point $\gamma_y = \gamma_x = b/2$. The critical value of b is $b_{cr} = -2(2j - 1)/(2j - 2)$, which is $b_{cr} < -2$ for finite systems and $b_{cr} \rightarrow -2$ in the thermodynamic limit. As already discussed, at the points $\gamma_x = \gamma_y$ the LMG Hamiltonian is diagonal in the basis $|jm = (-j + 2k)\rangle \propto (a^\dagger a^\dagger)^{(j-k)}(b^\dagger b^\dagger)^k|0\rangle$, with eigenvalues given by (16). The energies $E_{jm=-j}$ and $E_{jm=(-j+2)}$ cross at $\gamma_x = \gamma_y = -(2j - 1)/(2j - 2)$. Therefore, the line $\gamma_y = -\gamma_x + b_{cr}$ traverses a point at which the positive parity states $|jm = -j\rangle$ and $|j, m = -j + 2\rangle$ are degenerated.

Fig. 5.a shows the behavior of the 10 pairons in the interval $0.5 \leq t \leq 1.0$ for the three values of b . In the three cases the behavior of the nine lowest pairons is similar, all of them converging to -1 in the limit $t \rightarrow 1$. However, the last pairon close to $t = 1$ distinguishes clearly the three cases studied. For $b > b_{cr}$ the last pairon converges to -1 like the other nine pairons, whereas for $b < b_{cr}$ the last pairon converges to $+1$. The critical $b = b_{cr}$ separates both regions. In this case the last pairon converges to $e_- = \frac{\sqrt{j(2j-1)-1}}{\sqrt{j(2j-1)+1}} \approx 0.865$ for $t = 1$. The second panel, Fig. 5.b, shows more clearly the behavior of the last pairon near $t = 1$ for $b = b_{cr}$ and $b < b_{cr}$. Here, the horizontal scale has been extended to $t > 1$ using the symmetry transformation (14) $[(g, t, e_\alpha) \rightarrow (g, 1/t, 1/e_\alpha)]$. While for $b < b_{cr}$ the last pairon changes continuously across the value of $t = 1$, for $b = b_{cr}$ a discontinuity in the last pairon at $t = 1$ occurs due to the crossing of positive parity states, jumping from $e_- \approx 0.865$ to $e_+ = (1/e_-) \approx 1.156$. The degeneracy at the point $\gamma_x = \gamma_y = b_{cr}/2$ is associated to the states $|jm = -j\rangle \propto (a^\dagger a^\dagger)^j|0\rangle$ and $|jm = (-j + 2)\rangle \propto (a^\dagger a^\dagger)^{(j-1)}(b^\dagger b^\dagger)|0\rangle$. As it can be inferred from the exact wave function(19), the limit $t \rightarrow 1^-$ with $b = b_{cr}$ produces the right eigenstate

$$|\Psi\rangle = (a^\dagger a^\dagger)^{(j-1)} \left(\frac{a^\dagger a^\dagger}{e_- + 1} + \frac{b^\dagger b^\dagger}{e_- - 1} \right) |0\rangle \propto |\Psi_-\rangle \equiv \frac{|jm = -j\rangle - |jm = (-j + 2)\rangle}{\sqrt{2}},$$

which is a linear combination of the two degenerated states. The limit $t \rightarrow 1^+$ (with the last pairon converging to $e_+ \approx 1.156$) produces the other degenerated state, $|\Psi_+\rangle \equiv (1/\sqrt{2})(|jm = -j\rangle + |jm = (-j + 2)\rangle)$, orthogonal to the previous one. In summary, when the system traverses the line $\gamma_y = \gamma_x$ along the line $\gamma_y = -\gamma_x + b_{cr}$ the ground state wave function presents a discontinuity, changing from $|\Psi_-\rangle$ to $|\Psi_+\rangle$.

In general, the first order phase transition along the line $\gamma_y = \gamma_x$ (with $\gamma_x < 1$) is due to the crossing of the states $|jm\rangle$ and $|j(m + 2)\rangle$. As it was illustrated above for the particular case of the states $|jm = -j\rangle$ and $|jm = (-j + 2)\rangle$, the behavior of the pairons near this line reflects these crossings by a discontinuity in their values. As a result, crossing the line $\gamma_y = \gamma_x$ (with $\gamma_x < 1$) implies a jump from a $|\Psi_{-m}\rangle$ ground

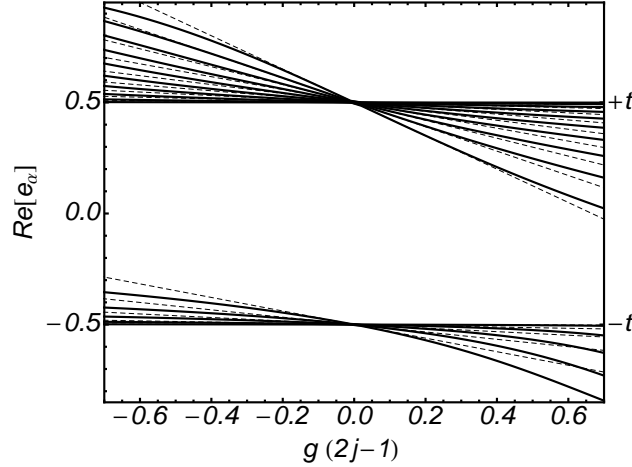


Figure 6: Pairons for the $k = 10$ -th positive parity excited state of a $j = 15$ system. The perturbative results (33) are shown by dashed lines and the exact ones with solid lines. The total number of pairons is $M = j = 15$. The $k = 10$ -th state is characterized by having 5 pairons close to $t_\alpha = -t$ and 10 pairons close to $t_b = +t$ at weak coupling. Note that the lower pairons for negative g are inside the interval $[-t, t]$, and the upper ones outside. The opposite happens for positive g where the lower pairons are outside the interval, and the upper pairons are inside.

state to a $|\Psi_{+m}\rangle$ ground state, where $|\Psi_{\pm m}\rangle \equiv \frac{1}{\sqrt{2}}(|jm\rangle \pm |j(m+2)\rangle)$. This first order phase transition is signaled by a discontinuous change in the order parameters $\langle S_x^2 \rangle$ and $\langle S_y^2 \rangle$. It can be shown that in the thermodynamic limit the order parameters for these states are

$$\begin{aligned} \frac{\langle \Psi_{\pm m} | S_x^2 | \Psi_{\pm m} \rangle}{j^2} &= \frac{2 \pm 1}{4} \left(1 - \left(\frac{m}{j} \right)^2 \right) \\ \frac{\langle \Psi_{\pm m} | S_y^2 | \Psi_{\pm m} \rangle}{j^2} &= \frac{2 \mp 1}{4} \left(1 - \left(\frac{m}{j} \right)^2 \right). \end{aligned} \quad (32)$$

Therefore, a jump from $|\Psi_{-m}\rangle$ to $|\Psi_{+m}\rangle$, for $m \neq -j$, produces a discontinuity in the order parameters characterizing a first order phase transition, in complete accord with the analysis of section 1. For the particular case of figure 5 ($m = -j$) both order parameters vanish at the critical point preventing a first order phase transition. The critical value for this continuous phase transition is $b_{cr} = -2(2j-1)/(2j-2) \rightarrow -2$ in the thermodynamic limit, corresponding to the triple point $\gamma_x = \gamma_y = -1$, in complete agreement with the thermodynamic results of reference [8]

5. Excited states in the hyperbolic LMG model

We will study in this section the excited states for the hyperbolic regions ($s = -1$) of the LMG model in terms of the pairon dynamics of the RG model. A similar description for the rational bosonic RG model was performed in [21]. Pairons for the rational as well as for trigonometric bosonic RG models are always real. The hyperbolic model has the particular feature that the pairons can take complex values. For the sake of clarity, let us assume the specific value $t = 1/2$, with generic results for the cases $t < 1$. The effective charges Q_C and Q_D of the Richardson equations (20) located at positions $P_C = -1$ and $P_D = 1$, are outside of the interval $[-t, t]$. The cases with $t > 1$, can be inferred from those with $t < 1$ through the mirror transformation of Eq. (14).

Let us first analyze the limit $g = 0$. In this limit the LMG Hamiltonian reduces to an one-body Hamiltonian $H = \epsilon S_z = \epsilon \frac{b^\dagger b - a^\dagger a}{2}$ with eigenvalues $\epsilon(n_b - n_a)/2$ and eigenstates $|\Psi\rangle = |n_b = \nu + 2k, n_a = \nu + 2(M - k)\rangle$. Here, the seniorities are the number of unpaired bosons $\nu = 0, 1$, $M = (j - \nu)$ is the total

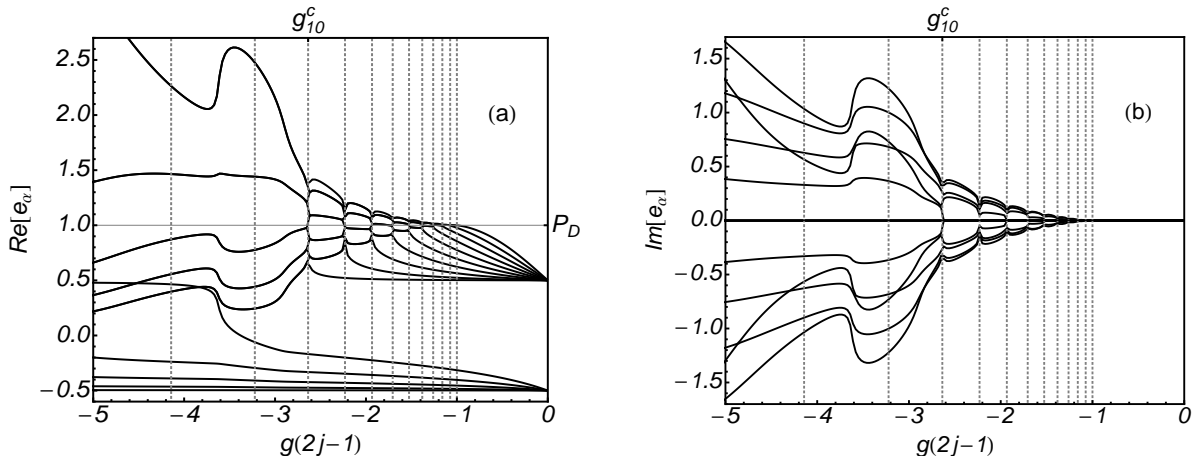


Figure 7: Real (a) and Imaginary (b) parts of the 15 pairons of the ($k = 10$) state of figure 6 as function of $g(2j - 1)$. Vertical dashed lines indicate the g values where pairon collapses occur according to Eq.(31). The pairons close to $t_a = -t$ in the weak coupling limit remain trapped in the real interval $[-t, t]$, whereas the non trapped pairons expand in the complex plane after collapsing in the position $P_D = 1$ [horizontal gray line in panel (a)] of the effective charge Q_D . The number of non trapped pairons for this 10-th excited state is 10, therefore collapses of 1 to 10 pairons occur at g values given, respectively, by $g = g_{N_D}^c$ with $N_D = 1, \dots, 10$. The results corresponding to $g_{N_D=10}^c$ are indicated in the upper scale of the panels. For $g < g_{N_D=10}^c$ no more collapses occur, and the pairon set consist of 5 real pairons in interval $[-t, t]$ and 5 complex conjugated pairon pairs.

number of boson pairs, and $k = 1, \dots, M$. The positive (negative) parity sector corresponds to n_a and n_b even (odd), or in terms of the seniorities it corresponds to $\nu = 0$ ($\nu = 1$). Independently of the parity, the ground state has M boson pairs occupying the a level. The excited states are obtained by promoting boson pairs from the a to the b level. In this way the k -th excited state for a given parity has $M - k$ boson pairs occupying the a level, and k in the b level. From the wave function (19), it can be seen that in the k -th excited state $M - k$ pairons converge to $t_a = -t$ and k pairons to $t_b = +t$. For finite but small g , it was shown in ref.[15] that the pairons e_α can be approximated by

$$e_\alpha \approx t_i - g(1 + st^2)r_l, \quad (s = -1) \quad (33)$$

where $t_i = t_a = -t$ or $t_i = t_b = +t$, and r_l are the positive roots of the Legendre polynomial $L_{N_i}^{\nu-1/2}(x)$, with N_i ($i = a, b$) the number of e_α pairons converging to t_i for $g = 0$, i.e, $N_a = M - k$ and $N_b = k$, for the k -th excited state. Hence, for small g , the entire set of states can be classified by the number of pairons distributed close to t_a and close to t_b . For the k -th excited state in the limit g negative and small, a group of $M - k$ pairons is close and above $t_a = -t$, implying they are in the interval $[-t, t]$, which will turn be very relevant for their behavior in larger g . A second group of k pairons is close and above $t_b = +t$, i.e. outside the interval $[-t, t]$. For small and positive g the situation is reversed. $M - k$ pairons are outside the interval $[-t, t]$ and close to $t_a = -t$, whereas the remaining k pairons are inside the interval and close to $t_b = +t$. In Figure 6 we illustrate this behavior for the positive parity 10-th excited state of a system with $M = j = 15$ pairons. In the figure, $k = 10$ pairons are close to $t_b = +t$ and the remaining $M - k = 5$ sit close to $t_a = -t$. Even if the perturbative result is not valid for large g , the behaviour of the pairons as a function of g is strongly dependent on their values at weak coupling. In particular on whether they are inside or outside the interval $[-t, t]$. The pairons inside the interval $[-t, t]$ expand in the real axis but remain constraint to it for any value of g . On the contrary, the pairons outside the interval expand on the real axis moving away from the interval. For negative g this expansion takes place above the interval $[-t, t]$ till the pairons start to collapse in the position $P_D = 1$ of the effective charge Q_D for values of g given by (31). Similar collapses occur for positive g for values given by (30), but here the collapses take place at the position $P_C = -1$ of the effective charge Q_C .

For positive values of g , the k -th excited state has $M - k$ pairon non trapped in the interval $[-t, t]$. Therefore, for the ground state ($k = 0$) all the pairons will successively collapse at $P_C = -1$ for increasing

g as it can be seen in figure 3. The first excited state has one pairon trapped in the interval $[-t, t]$, while the other $(M - 1)$ non trapped pairons successive collapse at $P_C = -1$ for increasing values of g . The same reasoning extends for the rest of the excited states. For the most excited state, with all its pairons trapped in the interval $[-t, t]$, no collapse occurs.

The situation is somewhat reversed for negative values of g . The k -th excited state has k non trapped pairons. Therefore, the higher the excited state is, the more collapses will occur in the position of effective charge Q_D at g values given by Eq. (31). For the ground state ($k = 0$), since all the pairons are trapped in the interval $[-t, t]$ no collapse occurs, as it can be seen in figure 3. For the k -th excited state successive collapses of 1 to k pairons occur at g values given, respectively, by $g_{N_D=1}^c, g_{N_D=2}^c, \dots, g_{N_D=k}^c$.

In Fig. 7 we illustrate this behavior for the same system and state of figure 6 ($P = +$, $j = 15$ and 10-th excited state), and for negative values of g . For small g , five pairons are located close and above $t_a = -t$ and $k = 10$ pairons are close and above $t_b = t$. As g is increased the trapped pairons expand in the interval $[-t, t]$, but remain constraint to it for any negative g . Whereas, the other ten pairons expand outside this interval, till they begin to collapse into the position ($P_D = 1$) of the effective charge Q_D at g values given by Eq.(31). These g values are indicated by vertical dashed lines in the panels of Fig. 7. Immediately after the collapse of an even number of pairons two complex conjugated pairons are created, and they expand in the complex plane until the next collapse. For the case illustrated in the figure, since the number of non trapped pairons is 10, the last collapse to $P_D = 1$ takes place at $g = g_{N_D=10}^c$. From there on five complex conjugated pairon pairs expand in the complex plane for $g < g_{N_D=10}^c$.

A better insight on the pairon dynamics can be gained by plotting the pairon positions in the two dimensional complex plane. Fig. 8 shows the pairon positions in the complex plane of the complete set of positive parity states for a system of $j = 30$ and two different negative g . The first one [panel (a)] is $g = g_{N_D=22}^c$ where $N_D = 22$ pairons collapse in $P_D = 1$. The second one [panel (b)] is an intermediate value of g between two collapses ($g_{N_D=23}^c < g < g_{N_D=22}^c$). The complex conjugated pairs of pairons of a given state are distributed in complex arcs around $P_D = 1$. In panel (a), the radius of these arcs goes to zero for states with large enough number of non-trapped pairons, i.e. for those states with $k = 22$ to $k = j = 30$ non trapped pairons, corresponding to the 22-th to 30-th excited state. In both cases the outer arcs correspond to less excited states.

Before closing this section, it is interesting to note that the condition (31) of N_D pairons converging to $P_D = 1$ in the hyperbolic region ($s = -1$) of phase diagram, defines hyperbolas in the γ_y - γ_x plane given by

$$\gamma_y \gamma_x = \left(\frac{2j - 1}{2j + 1 - 2N_D} \right)^2. \quad (34)$$

For $N_D = 1$, the resulting hyperbola ($\gamma_y \gamma_x = 1$) is the same reported in [8] for the crossing of the ground states of positive and negative parities in the third quadrant. Moreover, in [31] it is argued that the rest of the hyperbolas ($N_D = 2, \dots, M$) define the points where there are crossings between excited states of the two parity sectors. For instance, for $N_D = 2$ the ground and first excited state of positive parity cross, respectively, those of the negative parity sector. In general, for arbitrary N_D the corresponding hyperbola defines the points where the first N_D states of positive parity cross, respectively, the first N_D negative parity states. This result, already confirmed in [31, 32] for the ground state, is numerically confirmed here for the ground and excited states in figure 9. The figure displays the absolute value difference ($|E_{P+} - E_{P-}|$) between $P+$ and $P-$ states for a system with $j = 10$ and $t = 1/2$ as a function of negative g (third quadrant in the phase diagram $\gamma_x - \gamma_y$). The differences between the ground, first, second, third and fourth excited states of every parity sector are shown in logarithmic scale in order to make clear the crossings between positive and negative parity states. Every line is divided in continuous and dotted segments indicating if the difference $E_{P+} - E_{P-}$ is negative or positive respectively. The points where this difference changes sign indicate a crossing between positive and negative parity states. The vertical dashed lines signal the points where the hyperbolas (34) are traversed, i.e. when $g(2j - 1) = g_{N_D}^c(2j - 1) = -\frac{2j-1}{2j+1-2N_D}$. As it can be seen in the figure, for $N_D = 1$ [where $g(2j - 1) = -1$] the ground states of every parity sector cross, whereas for the leftmost vertical lines ($N_D = 2, 3, 4, 5$), in addition to the ground states, more and more excited states cross. It is worth mentioning that the phase transition in the thermodynamic limit is expected at

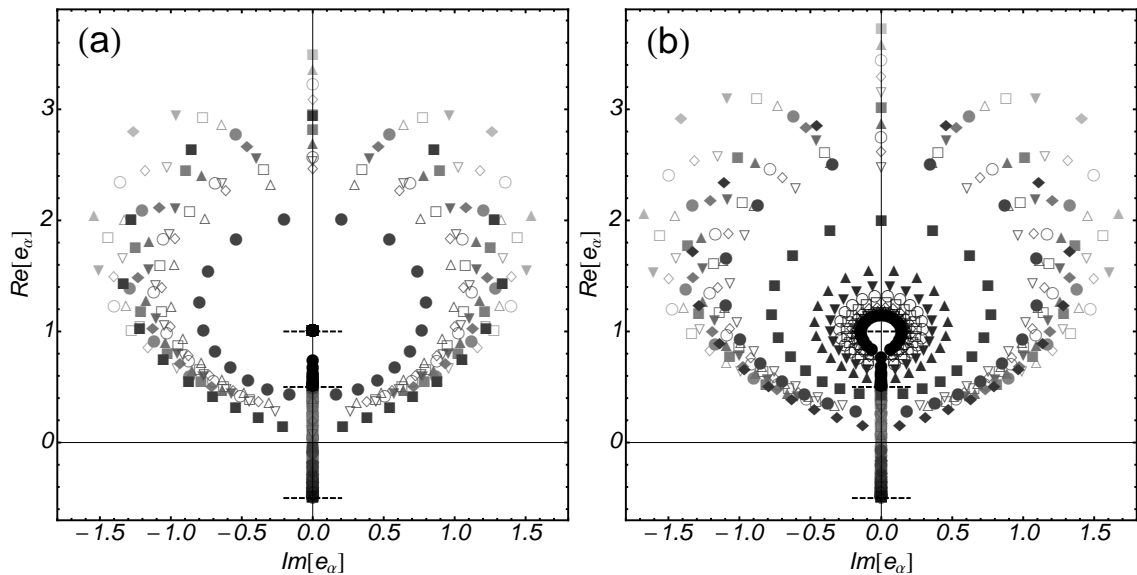


Figure 8: Pairons in the complex plane for the complete set of positive parity states for a $j = 30$ system. Panel (a) corresponds to $g = g_{S_2}^c$ where collapses of 22 pairons are expected according to Eq. (31). Panel (b) corresponds to a value of g where collapses are not expected. Horizontal dotted lines indicate the values $t = -1/2$, $t = 1/2$ and $P_D = 1$. The complex pairons of each state accommodate in arcs around $P_D = 1$. Outer arcs correspond to lower energy states. In panel (a) the arcs of the $k = 22$ to $k = j = 30$ excited state collapse to the position $P_D = 1$, with the outer arcs corresponding to lower energy excited states.

$g(2j - 1) = -t = -1/2$ (see table 2). We can appreciate in the figure a dramatic change in the difference between the energies of the positive and negative parity ground states around this value. However, the first crossing occurs at $g(2j - 1) = -1$.

A preliminary view to the relation between collapses and crossings of different parity states indicates that the states participating in a given crossing do not have their pairons collapsing in $P_D = +1$. Contrarily, the pairon collapses of a given state prevent it from having a crossing. As result, the ground state having no pairon collapses, has crossings for all the values $g_{N_D}^c$. By contrast, the most excited state with pairon collapses in every value $g_{N_D}^c$, does not have crossings. For intermediate states, they present crossings in $g = g_{N_D}^c$ only if for this particular value, their pairons do not present collapses. This condition occurs if N_D is greater than the number of their non trapped pairons (k for the k -th excited state). For instance, the 10-th $P = +$ excited state of Figure 7 cross the 10-th excited $P = -$ state only for $g_{N_D=11}^c, g_{N_D=12}^c, \dots, g_{N_D=j}^c$. Further research in this relation is desirable to establish a deeper connection between both phenomena, crossings and pairing collapses. Likewise, the hyperbolic quadrants of the phase diagram have a region where avoiding crossings between states of the same parity take place. This region already identified in [33] by studying the density of states in the thermodynamic limit, appears in the hyperbolic case ($s = -1$) when $|g(2j - 1)| > 1/t$. The relation between avoiding crossings and the pairon behavior in the $SU(1, 1)$ RG models is out of scope of this contribution, and deserves more work for a complete clarification.

6. Summary

The Schwinger boson representation of the $SU(2)$ algebra allows to connect the LMG model with the two-level $SU(1,1)$ RG pairing models. We have exploited this relation to classify the entire parameter space of the LMG model in terms of the three RG families, the rational, the trigonometric and the hyperbolic. This classification sheds new light into the LMG phase diagram and its quantum phase transitions. Moreover, the electrostatic mapping of the trigonometric and hyperbolic models provides new insights into the structure of the different phases. We explored the LMG model from the perspective of the RG models, where the

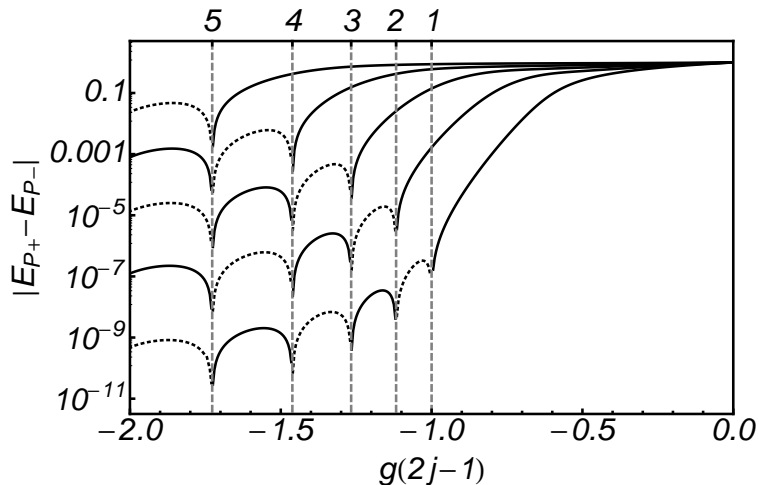


Figure 9: Absolute value of the difference between the ground to the fourth excited state energies of positive and negative parity states for the hyperbolic LMG model with $j = 10$ and $t = 1/2$. Continuous segments indicate that the $P = +$ state is lower in energy respect to the corresponding $P = -$ state, whereas the dashed segments correspond to the opposite situation $E_{P-} < E_{P+}$. The vertical dashed lines indicate the values $g_{N_D}^c$ (with $N_D = 1, \dots, 5$ signaled in the upper scale).

eigenstates are completely determined by the spectral parameters (pairons) of a particular solution of the non-linear set of Richardson equations. We proposed a numerically robust method to solve the Richardson equations which generalize that of reference [28]. The method was proven to be suitable for obtaining the pairons of the complete set of eigenstates for moderate systems sizes.

Using boson coherent states, we have re-derived the phase diagram of the LMG model and the characteristics of its different phase transitions. The second order phase transitions were interpreted in terms of the RG solution as a localization-delocalization of the ground state pairons, which takes place when the pairons concentrated around the value $t_a = -t$ at weak coupling, expand in the whole interval $[t_a, t_b] = [-t, t]$. On the other hand, the first order phase transition was related to the discontinuity of the pairons when the transition line is traversed. This discontinuity was related, in turn, with the crossings between states of the same parity. We have confirmed that the dynamics of pairons in the rational and trigonometric RG models take place entirely in the real axis. However, it was unexpected to find complex pairon solutions in the hyperbolic regions of the phase diagram. For the ground state, complex values of the pairons are obtained after the collapses of an even number of pairons into the position $P_C = -1$ of the effective charge Q_C . It was numerically verified diagonalizing very large systems that no phase transition is associated with this singular pairon behavior, even for the particular case in which all the pairons collapse into $P_C = -1$. For the latter case the ground state wave function has a particularly simple form which is equivalent to the Moore-Read state of the $p_x + ip_y$ model [18, 19, 20].

A complete classification of the excited states for the hyperbolic regions was given in terms of their pairon positions. For negative couplings it was found that the k -th excited state is characterized by a set of $(M - k)$ pairons trapped in the real interval $[-t, t]$ while the other k pairons lie outside this interval. The dynamics of these non trapped pairons show collapses of N_D pairons in the position $P_D = 1$ of the effective charge Q_D , at g values given by $g_{N_D}^c = -1/(2j + 1 - 2N_D)$. This singular behavior of the excited state pairons was found to be connected to the crossings of N_D lowest positive parity states with N_D negative parity states, at exactly the same values $g_{N_D}^c$. As discussed in Ref. [22], the pairon dynamics can help to identify significant physical phenomena. The relation between collapses and crossings is an example of this connection that deserves a deeper study. The collapses of pairons in the positions of the effective charges obtained in the hyperbolic boson RG models discussed here, is a feature also found in the $p_x + ip_y$ fermion pairing realization of the hyperbolic $SU(2)$ RG model [18, 19, 20]. In this latter model the collapses were related with another singular phenomenon: a third order phase transition. The insight gained in the study

of the LMG model, where the set of pairons of every state in the spectrum is easily accessible, can help to elucidate more intricate mechanisms in other integrable models where the numerical access to the pairon sets is more demanding.

Acknowledgements

J. D. acknowledges support from the Spanish Ministry of Economy and Competitiveness under grant FIS2009-07277.

References

- [1] H. J. Lipkin, N. Meshkov, and A. J. Glick, Nucl. Phys. **62**, 188 (1965).
- [2] P. Ring and P. Schuck, *The Nuclear Many Body Problem*, (Springer Verlag, New York, 1981).
- [3] R. Botet, R. Julien, and P. Pfeuty, Phys. Rev. Lett. **49**, 478 (1982).
- [4] R. G. Unanyan, and M. Fleischhauer, Phys. Rev. Lett. **90**, 133601 (2003).
- [5] J. Links, H. Q. Zhou, R. H. McKenzie, and M. D. Gould, J. Phys. A **36**, R63 (2003).
- [6] Chen G., Liang J.-Q., and Jia S., Opt. Express, **17**, 19682 (2009).
- [7] J. Larson, Europhys. Lett. **90**, 54001 (2010).
- [8] O. Castaños, R. López-Peña, J. Hirsch, and E. López-Moreno, Phys. Rev. B **74**, 104118 (2006).
- [9] J. Vidal, J. M. Arias, J. Dukelsky, and J. E. García-Ramos, Phys. Rev. C **73**, 054305 (2006).
- [10] J. Vidal, G. Palacios, and R. Mosseri, Phys. Rev. A **69**, 022107 (2004).
- [11] J. Vidal, J. Dukelsky, and R. Mosseri, Phys. Rev. A **69**, 054101 (2004).
- [12] W. D. Heiss, F. G. Scholtz, and H. B. Geyer, J. Phys. A **38**, 1843 (2005).
- [13] A. Relaño, J. M. Arias, J. Dukelsky, J. E. García-Ramos, and P. Pérez-Fernández, Phys. Rev. A **78**, 060102 (2008).
- [14] F. Pan, and J. P. Draayer, Phys. Lett. B **451**, 1 (1999).
- [15] G. Ortiz, R. Somma, J. Dukelsky, and S. Rombouts, Nucl. Phys. B **707**, 421 (2007).
- [16] J. Dukelsky, C. Eсеbbag, and P. Schuck, Phys. Rev. Lett. **87**, 066403 (2001).
- [17] J. Dukelsky, S. Pittel, and G. Sierra, Rev. Mod. Phys. **76**, 643 (2004).
- [18] M. Ibañez, J. Links, G. Sierra, and S.-Y. Zhao, Phys. Rev. B **79**, 180501 (2009).
- [19] C. Dunning, M. Ibañez, J. Links, G. Sierra, S.-Y. Zhao, J. Stat. Mech. P08025 (2010).
- [20] S. M. A. Rombouts, J. Dukelsky, and G. Ortiz, Phys. Rev. B, **82**, 224510 (2010).
- [21] J. Dukelsky and S. Pittel, Phys. Rev. Lett **86**, 4791 (2001).
- [22] D. Rubeni, A. Foerster, E. Mattei, and I. Roditi, Nucl. Phys. B **856**, 698 (2012).
- [23] P. Van Isacker, A. Frank, and J. Dukelsky, Phys. Rev. C **31**, 671 (1985).
- [24] J. Dukelsky, C. Eсеbbag, and S. Pittel, Phys. Rev. Lett. **88**, 062501 (2002).
- [25] J. M. Roman, G. Sierra, and J. Dukelsky, Nucl. Phys. B **634**, 483 (2002).
- [26] S. Rombouts, D. Van Neck, and J. Dukelsky, Phys. Rev. C **69**, 061303 (2004).
- [27] X. Guan, K.D. Launey, M. Xie, L. Bao, F. Pan, and J.P. Draayer, Phys. Rev. C **86**, 024313 (2012).
- [28] F. Pan, L. Bao, L. Zhai, X. Cui, and J.P. Draayer, J. Phys. A: Math. Theor. **44**, 395305 (2011).
- [29] A. Faribault, O. El Araby, C. Strater, and V. Gritsev, Phys. Rev. B **83**, 235124 (2011).
- [30] I. Marquette and J. Links, J. Stat. Mech., P08019 (2012).
- [31] O. Castaños, R. López-Peña, J. Hirsch, and E. López-Moreno, Phys. Rev. B **72**, 012406 (2005).
- [32] G. Chen and J-Q Liang, New Journal of Physics **8**, 297 (2006).
- [33] P. Ribeiro, J. Vidal, R. Mosseri, Phys. Rev. Lett. **99**, 050402 (2007).

Appendix A. Lamé differential equation from the RG equations

Here we show that the polynomial $P(x) = \prod_{\alpha=1}^M (x - e_{\alpha})$, with e_{α} being the roots of the Richardson equations, satisfies the Lamé differential equation. The demonstration is based on the simple identity

$$\frac{1}{(x-F)(x-G)} = \frac{1}{F-G} \left(\frac{1}{x-F} - \frac{1}{x-G} \right). \quad (\text{A.1})$$

From the definition of $P(x)$ it is straightforward to show that its derivative is $P'(x) = \sum_{\alpha=1}^M \prod_{\beta \neq \alpha} (x - e_{\beta})$. Therefore, we have the identity $\Lambda(x) \equiv P'(x)/P(x) = \sum_{\alpha} \frac{1}{x - e_{\alpha}}$. A derivative of $\Lambda(x)$ yields

$$\Lambda'(x) = \frac{P''(x)}{P(x)} - \Lambda^2(x) = - \sum_{\alpha} \frac{1}{(x - e_{\alpha})^2}.$$

From the previous result and the identity (A.1), we obtain

$$\frac{P''(x)}{P(x)} = -\sum_{\alpha} \frac{1}{(x-e_{\alpha})^2} + \sum_{\alpha} \frac{1}{x-e_{\alpha}} \sum_{\beta} \frac{1}{x-e_{\beta}} = \sum_{\alpha} \frac{2}{x-e_{\alpha}} \sum_{\beta \neq \alpha} \frac{1}{e_{\alpha}-e_{\beta}}.$$

Now, if e_{α} are the roots of the Richardson equations, the second sum in the right hand can be substituted according using Eq.(22)

$$\frac{P''(x)}{P(x)} = -\sum_{\alpha} \frac{2}{x-e_{\alpha}} \sum_k \frac{\rho_k}{e_{\alpha}-\eta_k} = \sum_k \frac{2\rho_k}{x-\eta_k} \sum_{\alpha} \left(-\frac{1}{x-e_{\alpha}} + \frac{1}{\eta_k-e_{\alpha}} \right),$$

where we have, again, used the identity (A.1). From the definition of $\Lambda(x)$ the previous equation is equivalent to

$$\frac{P''(x)}{P(x)} + \left(\sum_k \frac{2\rho_k}{x-\eta_k} \right) \frac{P'(x)}{P(x)} - \sum_k \frac{2\rho_k \Lambda(\eta_k)}{x-\eta_k} = 0.$$

Finally, multiplying the previous expression by $P(x)$ and $A(x) \equiv \prod_k (x-\eta_k)$, we obtain the Lamé differential equation (24),

$$A(x)P''(x) + \left[A(x) \sum_{k=1}^4 \frac{2\rho_k}{x-\eta_k} \right] P'(x) - \left[\sum_k 2\rho_k \Lambda(\eta_k) \prod_{l \neq k} (x-\eta_l) \right] P(x) = 0.$$

Appendix B. Condition to have N_C pairons converging in the position $P_C = -1$ of the effective charge Q_C in the hyperbolic LMG model

Let us assume that N_C pairons converge to $P_C = -1$. Therefore we expand them as $e_{\alpha} = -1 + \delta z_{\alpha}$, with $\alpha = 1, \dots, N_C$, and δ an infinitesimal parameter. In this limit the Richardson equations corresponding to $\alpha = 1, \dots, N_C$ separate in a term proportional to $1/\delta$ and terms of order $\mathcal{O}(\delta^0)$. Both terms have to cancel independently. The term proportional to $1/\delta$ reads

$$\frac{1}{\delta} \left(\frac{Q_C}{z_{\alpha}} + \sum_{\beta} \frac{1}{z_{\alpha}-z_{\beta}} \right) = 0 \quad \text{with } \alpha = 1, \dots, N_C.$$

Therefore, in order to have N_C pairons converging to $P_C = -1$ the previous set of equations has to have a solution. Following the lines of Appendix A, let us suppose a polynomial whose roots give the solution of the previous set of N_C equations, $P_{N_C}(z) = \prod_{\alpha=1}^{N_C} (z-z_{\alpha})$. If the set z_{α} solves the system of equations, it can be shown that the previous polynomial is a solution of the differential equation

$$zP_{N_C}''(z) + 2P_{N_C}'(z)Q_C = 0.$$

The general solution is $P_{N_C}(z) = \frac{Dz^{-2Q_C+1}}{1-2Q_C} + E$, with D and E integration constants. By comparing this solution with the initial assumption $[P_{N_C} = \prod_{\alpha=1}^{N_C} (z-z_{\alpha})]$, we obtain the conditions $D = (1-2Q_C)$ and $-2Q_C+1 = N_C$. From latter condition and the definition (21) of Q_C we finally obtain that the necessary condition to have N_C pairons converging into $P_C = -1$ is

$$g = g_{N_C}^c \equiv \frac{1}{2j+1-2N_C}.$$

Note that this condition applies to any eigenvector, ground or excited state. Following a similar reasoning it can be shown that the condition to have N_D pairons converging to $P_D = 1$ is $-2Q_D+1 = N_D$, from where the condition

$$g = g_{N_D}^a \equiv -\frac{1}{2j+1-2N_D}$$

follows. It is important to note that the latter condition is satisfied for negative g , whereas the former is for positive g .